1046 *Macromolecules* **2011**, *44*, 1046–1052
DOI: 10.1021/ma102087k

Macromolecules
ARTICLE

The Janus Character of Heterogeneous Dendritic Nanoparticles

J. A. Chute,[†,‡] C. J. Hawker,[†,‡,§] K. Ø. Rasmussen,[⊥] and P. M. Welch*[,⊥]

[†]*Materials Research Laboratory, University of California, Santa Barbara, California 93106, United States,*
[‡]*Department of Chemistry and Biochemistry, University of California, Santa Barbara, California 93106, United States,*
[§]*Materials Department, University of California, Santa Barbara, California 93106, United States, and*
[⊥]*Theoretical Division, Los Alamos National Laboratory, Los Alamos, New Mexico 87545, United States*

Received September 9, 2010; Revised Manuscript Received December 22, 2010

ABSTRACT: We present a computational and theoretical study of dendrimer-based nanoparticles composed of two linear chain types attached to the terminal groups of a core dendrimer. The chains were coupled to the dendritic core in both topologically Janus and alternating configurations. We find that a straightforward extension of the well-known scaling theory for the size of star polymers due to Daoud and Cotton works well for these classes of molecules. This suggests that the chains preferentially stretch radially from the molecular center. As a result, we find that topological connectivity alone suffices to ensure the stability of a Janus configuration. Chemical mismatch that drives phase separation in melts of these chains does not dramatically affect Janus structures when they are topologically constrained and can only produce frustrated conformations in alternating assemblies in the molecular weight range studied herein. We also demonstrate that contrast variation scattering experiments are ideally suited to detecting the presence of Janus structures. Specifically, we propose a scalar metric based upon contrast variation scattering studies on a single class of nanoparticles that can capture the extent of their Janus nature.

I. Introduction

The unique physical properties of Janus particles have motivated much of the research on their synthesis and properties since their initial fabrication by Casagrande et al.[1,2] in the late 1980s. Taking their name from the two-faced Roman god, Janus, this class of particles presents two chemically distinct faces that give rise to the enhanced interfacial activity initially predicted by Binks et al.[3] Combining this amphiphilic behavior with the functionality that may be imparted by the core particle opens possibilities for their use in many advanced applications. These potential uses include roles in electro-optics,[4−6] molecular targeting,[7] blend compatibilizers,[8−11] and drug delivery formulations.[12−17]

Numerous schemes for producing Janus particles exist and yield a variety of both organic and inorganic materials. Preparatory methods including phase separation,[18−20] controlled surface nucleation,[4,21−24] partial masking,[25−29] and Pickering emulsions,[30−37] lead to inorganic Janus particles that range in sizes between sub-ten nanometers to hundreds of micrometers in diameter. Depending upon the method involved in constructing these particles, their shapes may consist of isometric hemispheres or anisotropic geometries such as "dumbbells". Organic Janus particles are usually polymeric in nature and can derive from cross-linked latexes,[38] miktoarm star polymers,[39−42] or heterofunctional dendrimers. In contrast to their inorganic analogues, precise control over chemical structure and functional group placement within the material characterizes organic Janus particles. Thus, organic synthetic routes may provide greater control over size, shape, and functionality.

The use of dendrimers as a central platform for the construction of these hybrid nanostructures presents an especially high level of control over the resulting structure of Janus particles. Their well-defined, regularly branched structure gives them physical characteristics not commonly observed in other polymeric materials. Select properties, including near-monodispersity, the ability to host small molecules, and the presence of a large number of chain ends to which different moieties may be attached, have motivated the formulation of several synthetic routes to Janus particles with dendritic cores. A precise number of either small functional groups or oligomers can be attached to the central dendritic core, giving rise to unique supramolecular structures, as illustrated by the recent work of Percec et al.[43]

While several investigators have employed simulations to probe the assembly of Janus particles,[44−50] numerous questions revolving around their monomolecular properties remain outstanding. Establishing when polymeric particles are truly Janus, rather than homogeneously mixed, and how robust that arrangement is under varying environmental conditions presents a particularly interesting set of challenges. If the constituent chains possess affinity for the supporting solvent, two phenomena compete to dictate the extent of intermixing of the chains; conformational entropy drives mixing, while concentration gradients tend to stretch the chains radially outward. This competition may be expected to dominate in the spherical brushlike Janus particles resulting from attaching oligomers to a dendritic core. Considering the effect of chemical mismatch that leads to phase separation in bulk materials further complicates the picture. Hsu and coworkers[51] argue that, for the grafted linear chains that they studied, the concept of a true phase transition should not apply to finite-sized molecules. Rather, they found that the degree of mixing changed continuously for their systems. Voets and coworkers[52] found that Janus structures were obtained over a broad range of environmental conditions in their experimental study of mixed micelle particles, suggesting that chemical mismatch alone cannot account for the demixing. Carefully probing potentially Janus particles with experiments such as small-angle neutron scattering may yield insight into their structure. However, Fütterer and co-workers[53] noted that the analytical expression

*Corresponding author. E-mail: PWelch@LANL.gov.

 Published on Web 01/24/2011

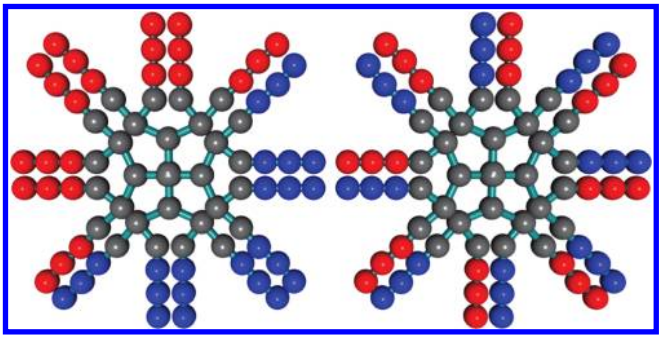

Figure 1. Two topologies considered in this study. The colors indicate different chain segment types. The left image represents a Janus connectivity while the right sketches an alternating assembly.

for the single particle scattering function of Janus spheres due to Kaya[54] predicts scattering very similar to that of core−shell species. They suggested a contrast variation approach to discern truly Janus structures from other candidate arrangements but relied upon comparisons with known mixed materials.

Herein, we apply Brownian dynamics simulations on coarse-grained models and arguments based on the scaling theory of Daoud and Cotton[55] to establish when a candidate Janus particle built upon a dendritic core actually manifests a two-faced structure. In particular, we present a robust recipe for measuring the extent of the Janus character from scattering experiments and demonstrate that, for attached oligomeric chains in a good solvent, chain stretching dominates; chemical mismatch need not play a role in producing Janus structures that are topologically constrained. We focus our attention on the case in which the particles, similar to block copolymers, may undergo conformational changes but maintain their chemical topology; no dynamic rearrangement in connectivity is allowed. In section II we present our simulation model and algorithm. Section III contains our predictions for the mass distribution within the molecule, a scaling argument for the radius of gyration, simulated contrast variation scattering experiments, our proposed scalar measure of the "Janusity" of a given particle, and the variation of that measure with chemical mismatch.

II. Simulation Model and Algorithm

We applied a coarse-grained model similar to that used by Zhou and Chen[56,57] in their studies of dendrimers with a single type of chain attached. Figure 1 illustrates the topologies examined. The red and blue chains denote two different chemical species and are attached in either a Janus configuration (shown left) or an alternating arrangement (shown right). The model dendrimer consists of a tetrafunctional core with dendrons that branch after each bond step. In our notation, Figure 1 contains two generation 3 dendrimers ($G = 3$) with trimer ($N_C = 3$) chains attached; we label a simple star polymer as generation 1, for example.

As in a previous study[58] of coarse-grained dendrimers, each bead in our model obeys the Langevin[59] equation of motion given by eq 1.

$$\frac{\mathrm{d}^2\vec{R}}{\mathrm{d}t^2} = -\xi\frac{\mathrm{d}\vec{R}}{\mathrm{d}t} - \vec{\nabla}U + \vec{f} \tag{1}$$

Here, R is the position in space, t is the simulation time, ξ is the frictional coefficient that captures the viscous drag on the bead exerted by the implicit solvent, U is the potential energy of the bead due to all of the other components of the molecule, and f is a random force that mimics the coupling of the molecule to the motion of the solvent with thermal energy kT. We only report ensemble average values in this paper and have made no effort to tie our model to any specific chemistry or solvent; the variable t may be simply viewed as a measure of the progress of the simulation. The frictional coefficient ξ was set to unity, and the expression for the potential energy U is discussed in detail below. The random force f is only locally correlated in time, obeying eq 2, and averages to zero.

$$\langle\vec{f}(t_0)\cdot\vec{f}(t_1)\rangle = 6kT\xi\delta(t_0 - t_1) \tag{2}$$

We used the velocity-Verlet algorithm to integrate the equation of motion forward in time, applying a time step $\Delta t = 0.004$. The random force f was drawn from the Maxwell−Boltzmann distribution given by eq 3 using the Box−Muller[60] method.

$$W(\vec{f}) = \left(\frac{1}{4\pi\xi kT}\right)^{3/2}\exp\left[\frac{-f^2}{4\xi kT}\right] \tag{3}$$

Simulations were typically run for 12−250 million time steps and samples saved at a frequency of 1 every 25 000 time steps.

Equation 4 describes the total system potential energy U and consists of two types of contributions. A simple harmonic potential maintains the connectivity of the model and is represented by the first sum in eq 4. The equilibrium bond length b_0 sets the length scale for the simulations, and all other lengths are reported in units of it. Every bond in the model is identical, and each bond length b_k fluctuates about b_0. To facilitate rapid relaxations within the models, the spring constant K was set to intermediate stiffness with $Kb_0^2/kT = 172.9$. If any bond length exceeded $1.43b_0$ during the course of a simulation (a very rare occurrence, only observed 2−5 times during the study), the calculations were halted and the results discarded to prevent the occurrence of nonphysical bond crossing.

$$U = K\sum_{k=1}^{N-1}(b_k - b_0)^2 + \sum_{i,j=1}^{N}\sigma_{i,j}[(\exp[-\alpha(R_{ij} - d)] - 1)^2 - 1] \tag{4}$$

The second term, a Morse potential, captures the nonbonded pairwise interactions between segments i and j separated by a distance R_{ij}. The range parameter α and the bead diameter d were fixed such that for all classes of interactions $\alpha b_0 = 16.8$ and $d/b_0 = 1.14$. However, the strength parameter $\sigma_{i,j}$ varied depending upon the identities of beads i and j. If both beads were of the same type (both red, both blue, or both black according to our color scheme in Figure 1), then $\sigma_{i,j}/kT = 1.18$. Similarly, both chain types (blue and red) interacted with the dendritic segments (black) with $\sigma_{i,j}/kT = 1.18$. This ratio ensures that the chains are behaving as though they are in a good solvent. To mimic chemical mismatch, however, the value of $\sigma_{i,j}/kT$ is treated as a variable falling between 0.12 and 1.18 when considering interactions between linear chain segments of different flavor (red−blue interactions). For simplicity, we drop the subscripts hereafter when discussing interchain interactions and simply denote the strength divided by the thermal energy as σ/kT. Clearly, when $\sigma_{i,j}/kT = 1.18$, the chains are identical. Values less than 1.18 drive a dissociation of the two bead types that produces phase separation in simple simulations containing only collections of linear chains. The generation number of the dendrimer G varied from 2 to 5 in our study, while the number of beads in the linear chains (all of identical length within the molecule) ranged from 20 to 200.

III. Results and Discussion

A. Mass Distribution. Examining the distribution of mass around the topological center of the molecule, the root

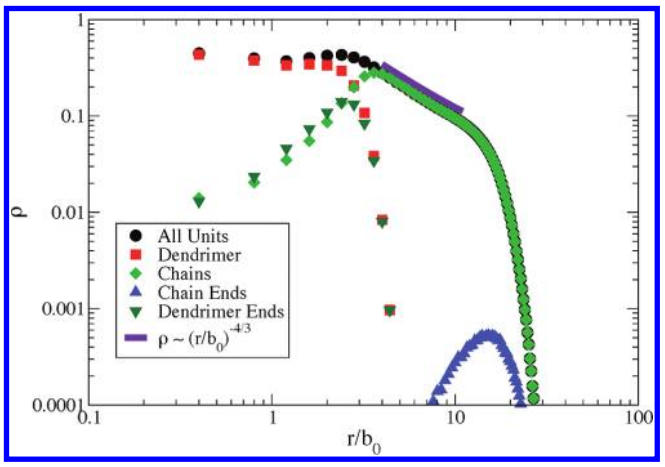

Figure 2. Mass distribution ρ as a function of distance from the center of the molecule. Data for $G = 5$ and $N_c = 100$ homopolymer case where all $\sigma_{i,j}/kT = 1.18$. Plots for the various molecular components are given as well as a power law curve showing the expected dependency predicted from Daoud and Cotton.

monomer, instructs us not only about the ability of the grafted dendrimer to host small molecules but also about the applicability of the Daoud and Cotton[55] theory for star polymers. We calculated this distribution $\rho(r)$ for the entire molecule, the dendrimer segments, the chain segments, the dendrimer−chain junction points, and the chain ends using eq 5.

$$\rho(r) = \frac{V_b}{V(r)}\langle n(r)\rangle \tag{5}$$

To do this, we divided space around the center of the molecule into a set of concentric shells. Here, V_b is the volume of a bead in our model, $V(r)$ is the volume of a shell falling at a distance r away from the center of the molecule, and $\langle n(r)\rangle$ is the average number of segments found in that shell.

Figure 2 contains the mass distributions for the homopolymer case ($\sigma_{i,j}/kT = 1.18$ for all i and j) with $G = 5$ and $N_c = 100$. The results were similar for all other configurations examined. The total mass distribution displays three different regimes of behavior. Dendrimer segments comprise the majority of the core region. However, some chain segments penetrate this domain, resulting in a diffuse boundary between regions rich in dendrimer segments and those rich in linear chain segments. This behavior is expected since, as also presented in Figure 2, the junction points between the dendrimer and chains are distributed throughout the core region, similar to the distribution of terminal units reported for unmodified dendrimers. As found by Zhou and Chen,[56,57] the chains also perturb the core dendrimer, swelling it slightly. Note that we are studying relatively compact dendritic structures herein with branching occurring after each new bond. One may expect greater back-folding by introducing greater flexibility into the model by placing beads between the branching points. Moving outward from the center of the molecule, the next region is dominated by chain segments. We present the data in Figure 2 on a log−log scale to illustrate that this region is consistent with the power law $\rho(r) \sim r^{-4/3}$. Though the range of the data is limited, this consistency reflects the behavior of swollen blobs composed of self-avoiding chain segments, as argued by Daoud and Cotton[55] for star polymers. The outermost region captures the rapid decline in mass, producing a nearly crisp molecular boundary on average.

B. Radius of the Molecule. Thus, informed about the mass distribution, we can calculate the relationship between the radius of the entire molecule R, the generation of growth G for the dendrimer, the molecular weight of the dendrimer N_D, the molecular weight for an individual chain N_C, and the number of chains attached F. To accomplish this, we follow closely the scaling prescription given by Daoud and Cotton.[55] The radial integral over the number of segments per volume in each shell up to the limiting radius of the molecule is proportional to the total mass ($N_D + N_C F$), as given by eq 6.

$$b_0{}^3 \int_0^R \frac{n(r)}{V(r)} r^2 \, dr \propto b_0{}^3 (N_D + N_C F) \tag{6}$$

We may decompose this integral into two regions, the first corresponding to the dendrimer-rich space and the other to the swollen chains, as captured by eq 7.

$$b_0{}^3 \int_0^R \frac{n(r)}{V(r)} r^2 \, dr \propto b_0{}^3 \int_0^{R_D} \frac{n(r)}{V(r)} r^2 \, dr + b_0{}^3 \int_{R_D}^R \frac{n(r)}{V(r)} r^2 \, dr \tag{7}$$

The first integral ranges from the center of the molecule to the radius of the dendrimer R_D and is clearly proportional to the mass of the dendrimer N_D. The second integral ranges from R_D to the radius of the entire molecule R. As shown by Daoud and Cotton[55]

$$b_0{}^3 \int_{R_D}^R \frac{n(r)}{V(r)} r^2 \, dr \propto b_0{}^{4/3} \nu^{-1/3} F^{2/3} \int_{R_D}^R r^{2/3} \, dr \tag{8}$$

in this region, where ν is the unitless excluded volume parameter. Here, we assume that each shell contains only F blobs, implying that the chains are stretched outward with little back-folding of the blobs. As shown by the mass distribution of the chain ends plotted in Figure 2, this is a reasonable approximation. Sheng[61] and co-workers showed that the radius of a dendrimer obeys eq 9.

$$R_D \propto b_0 \nu^{1/5} N_D{}^{1/5} G^{2/5} \tag{9}$$

Kröger and co-workers provide a generalization of this expression as well as a useful discussion of the limitations of scaling arguments to dendritic molecules.[62] While the dendrimers are slightly stretched by the presence of the chains, this proves to be good approximation here. Combining eqs 6−9 yields eq 10, the scaling relationship between the radius of the entire molecule R and the various molecular parameters.

$$R \propto b_0 \nu^{1/5} [N_D{}^{1/3} G^{2/3} + N_C F^{1/3}]^{3/5} \tag{10}$$

Figure 3 contains the root-mean-squared radius of gyration R_G normalized by the average bond length b_0 plotted against $[N_D{}^{1/3} G^{2/3} + N_C F^{1/3}]^{3/5}$ for all configurations studied. This includes data with G ranging from 2 to 5, N ranging from 20 to 200, and σ/kT ranging from 0.12 to 1.18. That this simple treatment captures the data tells us that the central approximation is faithful; there are roughly F blobs in each shell, suggesting that the chains do preferentially radiate outward rather than mix laterally. This holds significant implications about the robustness of Janus configurations.

C. Small-Angle Scattering Properties. Figure 4 contains snapshots of a Janus $G = 5$, $N_C = 200$ molecule with

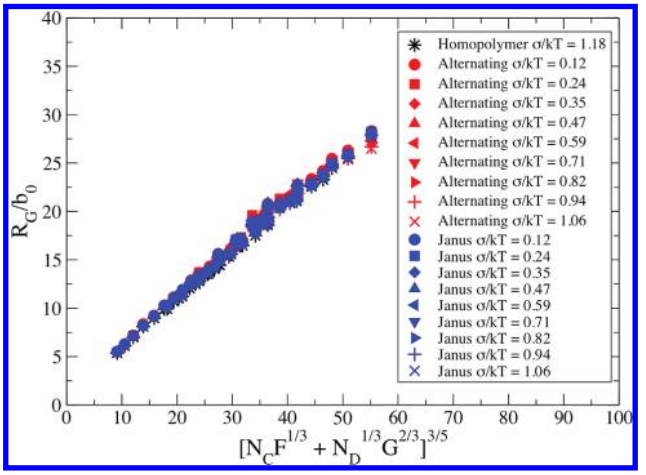

Figure 3. Root-mean-squared radius of gyration R_G normalized by the equilibrium bond length plotted as a scaling function of the molecular weight of the attached chains N_C, the number of attached chains F, the molecular weight of the dendrimer core N_D, and the generation of growth for that core G. Averages from all 418 distinct molecular configurations are shown, corresponding to 76 combinations of G, N_C, and pair interaction strength σ/kT.

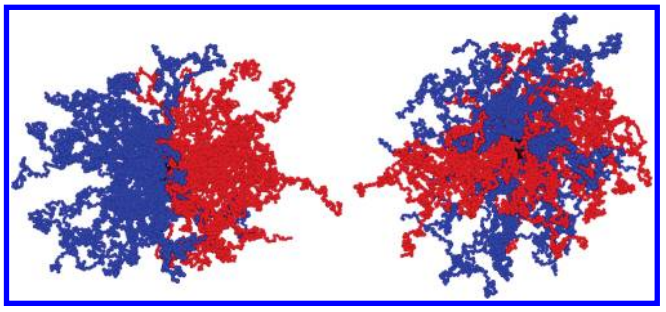

Figure 4. Typical snapshots from the simulations. The left image is that of a Janus configuration, and the right is that of an alternating assembly. Both molecules have $G = 5$, $N_C = 200$ with $\sigma/kT = 0.12$.

$\sigma/kT = 0.12$ as well as its alternating counterpart. Visual inspection permits classification of the molecules into either Janus or not but does not provide a sound discriminator of the extent of the segregation of the chains. Nor is it conveniently applied to real experimental systems (though use of microscopy may be imagined). Following Fütterer[53] and coworkers, we simulated contrast variation scattering experiments using eq 11.

$$I(\vec{q}) = \langle | \int (\Gamma - \Gamma_0) e^{-i\vec{r}\vec{q}} \, d\vec{r} \, |^2 \rangle \qquad (11)$$

Here, Γ is the local scattering length density, Γ_0 is the solvent scattering length density, and $I(q)$ is the calculated scattering intensity at wave vectors of magnitude q. The angular brackets denote ensemble averages over molecular conformation as well as rotation. Each snapshot was centered within a box that was further decomposed into cubes of size $(\Delta X/b_0)^3 = 1.0$. The local scattering length density Γ was calculated as the volume fraction weighted average of the bare scattering length densities of each component in the box, $\Gamma = \phi_R\gamma_R + \phi_B\gamma_B + \phi_D\gamma_D + \phi_S\Gamma_0$. Here, ϕ_R, ϕ_B, ϕ_D, and ϕ_S are the local volume fractions of the red chains, blue chains, dendrimer, and solvent, respectively. The scattering length densities of each component of the molecule will depend upon the details of the chemistry but are here assigned to be $\gamma_R = 0.0$, $\gamma_B = 1.0$, and $\gamma_D = 0.5$ in arbitrary units to maximize contrast. The value of Γ_0 was varied from 0 to 1.0, mimicking changes in the ratio of deuterated to nondeuterated solvent components.

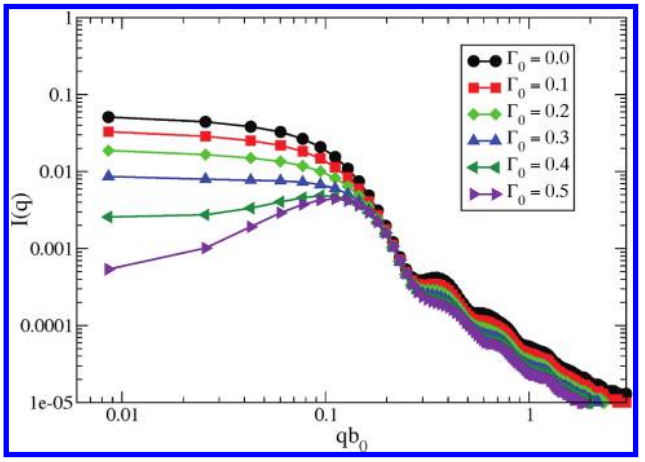

Figure 5. Calculated scattering intensity $I(q)$ in arbitrary units as a function of scattering vector magnitude q times the equilibrium bond length b_0. Data shown for a $G = 5$, $N_C = 100$ molecule with $\sigma/kT = 0.12$ in a Janus configuration. The solvent scattering length density Γ_0 was varied, mimicking a contrast variation experiment.

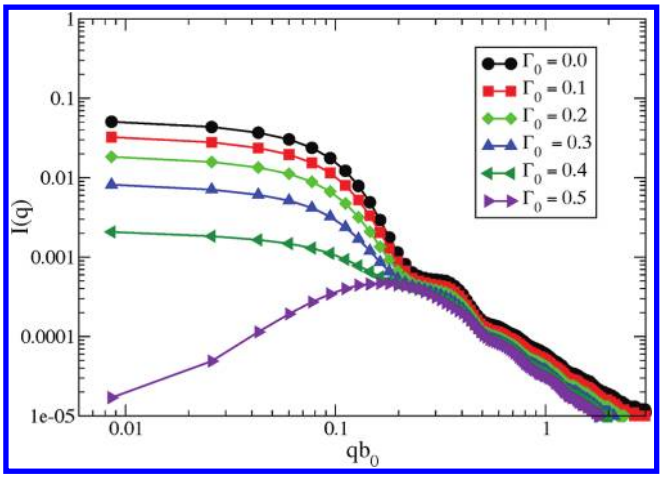

Figure 6. Calculated scattering intensity $I(q)$ in arbitrary units as a function of scattering vector magnitude q times the equilibrium bond length b_0. Data shown for a $G = 5$, $N_C = 100$ molecule with $\sigma/kT = 0.12$ in an alternating configuration. The solvent scattering length density Γ_0 was varied, mimicking a contrast variation experiment.

Figure 5 contains plots of the calculated scattering intensity as a function of qb_0 for $G = 5$, $N_C = 100$, and $\sigma/kT = 0.12$ in a Janus configuration. The solvent scattering length density is varied from 0.0 to 0.5, corresponding to moving from maximum contrast to a near-contrast matched state. Note that, due to the symmetry of the particles studied, the plots of scattering intensity for systems with solvent scattering length densities ranging from 0.6 through 1.0 exactly overlay those presented in Figure 5. Similarly, Figure 6 contains analogous data ($G = 5$, $N_C = 100$, and $\sigma/kT = 0.12$) for a molecule arranged in an alternating configuration. Clearly, simply comparing the scattering profiles of these two classes of molecules in the limit of maximum contrast ($\Gamma_0 = 0.0$) is insufficient to distinguish one from the other. However, in the limit of the near contrast-matched state, the alternating configuration shows a much lower drop in scattering intensity at low q than does the Janus architecture. This occurs because the alternating case results in local mixing of the two chain types to produce an average value of Γ closer to Γ_0. As pointed out by Fütterer[53] for the case of

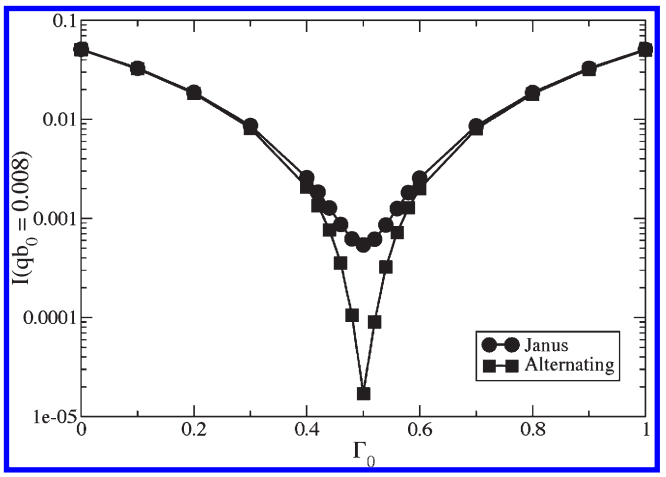

Figure 7. Calculated scattering intensity I in the low qb_0 limit in arbitrary units as a function of the solvent scattering length density Γ_0. Data shown for $G = 5$, $N_C = 100$ molecules with $\sigma/kT = 0.12$ in both Janus and alternating configurations.

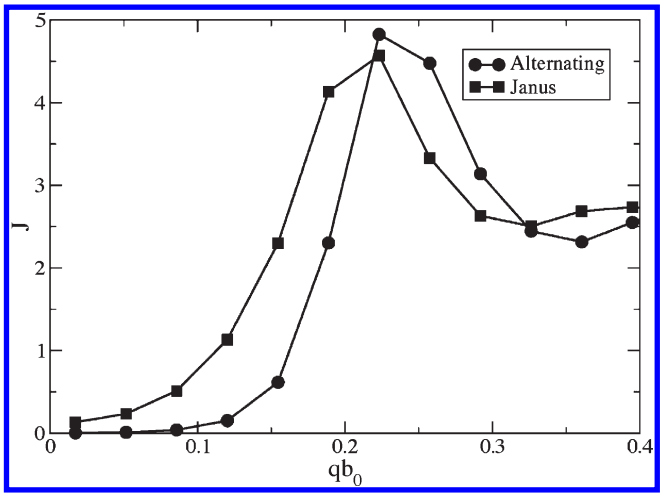

Figure 8. Janusity measure J as a function of the scattering vector magnitude q times the equilibrium bond length b_0. Data shown for the Janus and alternating configuration cases with $G = 5$, $N_C = 125$, and $\sigma/kT = 0.12$.

micelles, this signature is made clear when the scattering intensity taken from the low-q limit is plotted as a function of Γ_0 for the two types of molecules. This is illustrated in Figure 7 with data taken from Figures 5 and 6 at $qb_0 = 0.008$.

Unfortunately, producing a pair of molecules in both the Janus and alternating configurations is challenging, and we need a measure that does not depend upon such a comparison. We propose formulating a single scalar measure from the scattering intensities obtained at the extremes of the contrast range and its midpoint. In our model, this corresponds to $\Gamma_0 = 1$, 0, and 0.5. We define the "Janusity measure" $J(\vec{q})$ by eq 12.

$$J(\vec{q}) = \frac{I_1(\vec{q}) + I_0(\vec{q}) + 2I_{0.5}(\vec{q})}{I_1(\vec{q}) + I_0(\vec{q}) - 2I_{0.5}(\vec{q})} - 1 \qquad (12)$$

Here, $I_x(\vec{q})$ denotes the scattering intensities at the specified values of Γ_0. Ideally, $J(\vec{q})$ varies from nearly one in the limit of perfectly Janus molecules to zero for perfectly mixed (alternating) structures. However, as in the approach used in Figure 7, the precise value of q sampled affects the power of $J(\vec{q})$ to differentiate between Janus and mixed states.

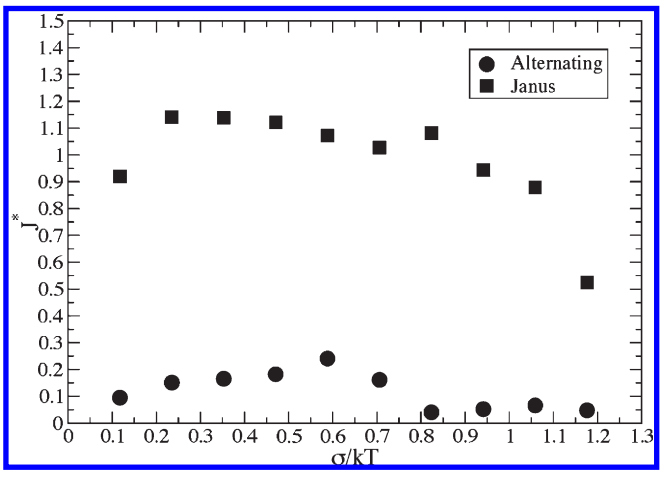

Figure 9. Characteristic Janusity J^* measured at the qb_0 values corresponding to 2 times the radius of gyration of each molecule plotted as a function of the pair wise interaction strength σ normalized by the thermal energy kT. Data for both the Janus and alternating configurations with $G = 5$ and $N_C = 125$ are shown.

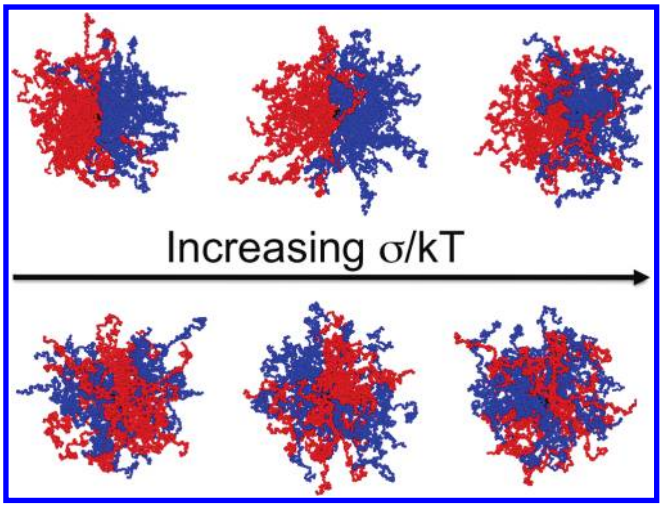

Figure 10. Typical snapshots from simulations of molecules with $G = 5$ and $N_C = 125$. The images in the top row are taken from simulations of Janus molecules, while those on the bottom are images of alternating configurations. The pairwise interaction strength σ divided by thermal energy kT increases from left to right with $\sigma/kT = 0.12$, 0.59, and 1.18.

Figure 8 contains plots of $J(\vec{q})$ vs qb_0 for the cases of $G = 5$, $N_C = 125$, $\sigma/kT = 0.12$ in both alternating and Janus configurations. In the high qb_0 limit, $J(\vec{q})$ is nearly identical for both configurations. However, in the lower qb_0 limit, as qb_0 approaches the range corresponding roughly to the diameter of the particles, $J(\vec{q})$ begins to effectively differentiate between the two structures. We therefore choose qb_0 that exactly corresponds to $1.3 \times 2 \times R_G$ and label it J^*. This choice of qb_0 is appropriate since it effectively probes length scales over which the two structures will most clearly differ in the distribution of the two chain types. The factor of 1.3 reflects the relationship between the R_G and the hydrodynamic radius of particles with radially decaying density profiles.

D. Importance of Phase Separation. Thus, armed with a standard measure of Janus character, J^*, we probed the importance of chemical mismatch by varying σ/kT from 0.12 to 1.18 for both Janus and alternating configurations. Figure 9 contains a plot of J^* over this range for both cases with $G = 5$ and $N_C = 125$. As expected, the

Janus configuration produces values of J^* uniformly larger than those for the alternating case. We also note that the value of J^* varies little over the range of σ/kT values studied, only decreasing in the limit of no chemical mismatch ($\sigma/kT = 1.18$). Thus, we find that chains attached in a Janus topological configuration result in a Janus nanosphere independent of the chemical mismatch between the two chain types; phase separation is not needed to achieve a Janus structure. Similarly, the alternating configuration produces values of J^* that always fall near zero. Snapshots from the simulations clearly illustrate these trends and are shown in Figure 10. The frustrated structures that result from chemical mismatch in the alternating configurations show that patchy spheres can be obtained by randomly attaching chains of different types. However, for the relatively short chains studied here, they still do not quite achieve truly Janus conformations.

IV. Conclusions

Janus nanoparticles hold potential for a number of applications, both in the bulk state and in heterogeneous systems. However, several questions about their structural development remain outstanding. Here, we provide a straightforward recipe for quantifying the Janus character of a nanoparticle using contrast variation scattering experiments. Specifically, we propose a unique scalar metric that utilizes neutron scattering intensities and falls to one for perfect Janus structures and zero for perfectly mixed configurations. We have focused on Janus nanoparticles built around spherical dendrimer templates since they hold promise for a higher degree of architectural control. However, our proposed measure of Janus character may also prove of value for a wide range of other Janus materials with nonspherical geometry, such as cylindrical Janus dendronized polymers.[63,64] Considering the topology studied herein, we employed a scaling argument similar to the Daoud and Cotton blob model for star polymers to successfully capture the relationship between the molecular parameters and the overall radius of gyration of the nanoparticle. This scaling prediction assumes that the chains stretch radially away from the core of the molecule, with little back-folding. We applied both this scaling theory and the neutron scattering metric to coarse-grained simulations of Janus and alternating nanoparticles with dendrimer cores. The ability of this scaling theory to encapsulate all of our numerical results coupled with results from the neutron scattering metric reveals a surprising relationship between the resulting overall structure and molecular topology; topological control alone can ensure the formation of Janus structures when the component chains are in a good solvent, regardless of the chemical composition. This implies that Janus structures can be formulated even if there is little chemical difference between the constituent chains and that a broad range of chemistries may be expected to result in two-faced nanoparticles with creative synthetic routes that impose topological control.

Acknowledgment. This work was carried out under the auspices of the National Nuclear Security Administration of the U.S. Department of Energy at Los Alamos National Laboratory under Contract DE-AC52-06NA25396. Financial support was provided by the U.S. Department of Energy Office of Biological and Environmental Research under Proposal SCFY081004, the Los Alamos National Laboratory Institute for Multiscale Materials Studies, and the National Science Foundation (CHE-054031 and MRSEC Program DMR-05204156 (MRL-UCSB)).

References and Notes

(1) Casagrande, C.; Veyssié, M. *C. R. Acad. Sci. Paris* **1988**, *306*, 1423.
(2) Casagrande, C.; Fabre, P.; Raphaël, E.; Veyssié, M. *Europhys. Lett*. **1989**, *9*, 251.
(3) Binks, B. P.; Fletcher, P. D. I. *Langmuir* **2001**, *17*, 4708.
(4) Behrend, C. J.; Anker, J. N.; Kopelman, R. *Appl. Phys. Lett*. **2004**, *84*, 154.
(5) Nisisako, T.; Torii, T.; Takahashi, T.; Takizawa, Y. *Adv. Mater*. **2006**, *18*, 1152.
(6) Kim, S.-H.; Jeon, S.-J.; Jeong, W. C.; Park, H. S.; Yang, S.-M. *Adv. Mater*. **2008**, *20*, 4129.
(7) Gillies, E. R.; Fréchet, J. M. J. *Drug Discovery Today* **2005**, *10*, 35.
(8) Hawker, C. J.; Wooley, K. L.; Fréchet, J. M. J. *J. Chem. Soc., Perkin Trans. 1* **1993**, 1287.
(9) Xu, H.; Erhardt, R.; Abetz, V.; Müller, A. H. E.; Goedel, W. A. *Langmuir* **2001**, *17*, 6787.
(10) Glaser, N.; Adams, D. J.; Böker, A.; Krausch, G. *Langmuir* **2006**, *22*, 5227.
(11) Walther, A.; Hoffmann, M.; Müller, A. H. E. *Angew. Chem., Int. Ed*. **2008**, *47*, 711.
(12) Jansen, J. F.; de Brabander-van den Berg, E. M.; Meijer, E. W. *Science* **1994**, *266*, 1226.
(13) Esfand, R.; Tomalia, D. A. *Drug Discovery Today* **2001**, *6*, 427.
(14) Cloninger, M. *Curr. Opin. Chem. Biol*. **2002**, *6*, 742.
(15) Stiriba, S.-E.; Frey, H.; Haag, R. *Angew. Chem., Int. Ed*. **2002**, *41*, 1329.
(16) Aulenta, F.; Hayes, W.; Rannard, S. *Eur. Polym. J*. **2003**, *39*, 1741.
(17) Dufés, C.; Uchegbu, I.; Schätzlein, A. G. *Adv. Drug Delivery Rev*. **2005**, *57*, 2177.
(18) Giersig, M.; Ung, T.; Liz-Marzán, L. M.; Mulvaney, P. *Adv. Mater*. **1997**, *9*, 570.
(19) Gu, H.; Zheng, R.; Zhang, X.; Xu, B. *J. Am. Chem. Soc*. **2004**, *126*, 5664.
(20) Lu, W.; Chen, M.; Wu, L. *J. Colloid Interface Sci*. **2008**, *328*, 98.
(21) Teranishi, T.; Inoue, Y.; Nakaya, M.; Oumi, Y.; Sano, T. *J. Am. Chem. Soc*. **2004**, *126*, 9914.
(22) Gao, X.; Yu, L.; Macuspie, R. I.; Matsui, H. *Adv. Mater*. **2004** *17*, 426.
(23) Yu, H.; Chen, M.; Rice, P. M.; Wang, S. X.; White, R. L.; Sun, S. *Nano Lett*. **2005**, *5*, 379.
(24) Li, Y.; Zhang, Q.; Nurmikko, A. V.; Sun, S. *Nano Lett*. **2005**, *5*, 1689.
(25) Bao, Z.; Chen, L.; Weldon, M.; Chandross, E.; Cherniavskaya, O.; Dai, Y.; Tok, J. B. H. *Chem. Mater*. **2002**, *14*, 24.
(26) Paunov, V. N. *Langmuir* **2003**, *19*, 7970.
(27) Paunov, V. N.; Cayre, O. J. *Adv. Mater*. **2004**, *16*, 788.
(28) Zhang, J.; Wang, X.; Wu, D.; Liu, L.; Zhao, H. *Chem. Mater*. **2009**, *21*, 4012.
(29) Anderson, K. D.; Luo, M.; Jakubiak, R.; Naik, R. R.; Bunning, T. J.; Tsukruk, V. V. *Chem. Mater*. **2010**, *22*, 3259.
(30) Takahara, Y. K.; Ikeda, S.; Ishino, S.; Tachi, K.; Ikeue, K.; Sakata, T.; Hasegawa, T.; Mori, H.; Matsumura, M.; Ohtani, B. *J. Am. Chem. Soc*. **2005**, *127*, 6271.
(31) Gu, H.; Yang, Z.; Gao, J.; Chang, C. K.; Xu, B. *J. Am. Chem. Soc*. **2005**, *127*, 34.
(32) Liu, B.; Wei, W.; Qu, X.; Yang, Z. *Angew. Chem., Int. Ed*. **2008**, *47*, 3973.
(33) Perro, A.; Meunier, F.; Schmitt, V.; Ravaine, S. *Colloids Surf., A* **2009**, *332*, 57.
(34) Hong, L.; Jiang, S.; Granick, S. *Langmuir* **2006**, *22*, 9495.
(35) Jiang, S.; Granick, S. *Langmuir* **2008**, *24*, 2438.
(36) Jiang, S.; Schultz, M. J.; Chen, Q.; Moore, J. S.; Granick, S. *Langmuir* **2008**, *24*, 10073.
(37) Jiang, S.; Chen, Q.; Tripathy, M.; Luijten, E.; Schweizer, K. S.; Granick, S. *Adv. Mater*. **2010**, *22*, 1060.
(38) Tanaka, T.; Okayama, M.; Kitayama, Y.; Kagawa, Y.; Okubo, M. *Langmuir* **2010**, *26*, 7843.
(39) Saito, R.; Fujita, A.; Ichimura, A.; Ishizu, K. *J. Polym. Sci., Part A: Polym. Chem*. **2000**, *38*, 2091.
(40) Erhardt, R.; Böker, A.; Zettl, H.; Kaya, H.; Pyckhout-Hintzen, W.; Krausch, G.; Abetz, V.; Müller, A. H. E. *Macromolecules* **2001**, *34*, 1069.
(41) Erhardt, R.; Zhang, M.; Böker, A.; Zettl, H.; Abetz, C.; Frederik, P.; Krausch, G.; Abetz, V.; Müller, A. H. E. *J. Am. Chem. Soc*. **2003**, *125*, 3260.
(42) Walther, A.; Matussek, K.; Müller, A. H. E. *ACS Nano* **2008**, *2*, 1167.
(43) Percec, V.; Wilson, D. A.; Leowanawat, P.; Wilson, C. J.; Hughes, A. D.; Kaucher, M. S.; Hammer, D. A.; Levine, D. H.; Kim, A. J.; Bates, F. S.; Davis, K. P.; Lodge, T. P.; Klien, M.; DeVane, R. H.; Aqad, E.; Rosen, B. M.; Argintaru, A. O.; Sienkowska, M. J.; Rissanen, K.; Nummelin, S.; Ropponen, J. *Science* **2010**, *328*, 1009.

(44) Erdmann, T.; Kröger, M.; Hess, S. *Phys. Rev. E* **2003**, *67*, 041209.
(45) Iacovella, C. R.; Horsch, M. A.; Zhang, Z.; Glotzer, S. C. *Langmuir* **2005**, *21*, 9488.
(46) Glotzer, S. C.; Horsch, M. A.; Iacovella, C. R.; Zhang, Z.; Chan, E. R.; Zhang, X. *Curr. Opin. Colloid Interface Sci.* **2005**, *10*, 287.
(47) Hong, L.; Cacciuto, A.; Luijten, E.; Granick, S. *Nano Lett.* **2006**, *6*, 2510.
(48) Iacovella, C. R.; Keys, A. S.; Horsch, M. A.; Glotzer, S. C. *Phys. Rev. E* **2007**, *75*, 040801.
(49) Iacovella, C. R.; Horsch, M. A.; Glotzer, S. C. *J. Chem. Phys.* **2008**, *129*, 044902.
(50) Iacovella, C. R.; Glotzer, S. C. *Nano Lett.* **2009**, *9*, 1206.
(51) Hsu, H.-P.; Paul, W.; Binder, K. *Macromol. Symp.* **2007**, *252*, 58.
(52) Voets, I. K.; Fokkink, R.; de Keizer, A.; May, R. P.; de Waard, P.; Cohen Stuart, M. A. *Langmuir* **2008**, *24*, 12221.
(53) Fütterer, T.; Vliegenthart, G. A.; Lang, P. R. *Macromolecules* **2004**, *37*, 8407.
(54) Kaya, H. *Appl. Phys. A: Mater. Sci. Process.* **2002**, *74*, S507.
(55) Daoud, M.; Cotton, J. P. *J. Phys.* (*Paris*) **1982**, *43*, 531.
(56) Zhou, T.; Chen, S. B. *Macromolecules* **2005**, *38*, 8554.
(57) Zhou, T.; Chen, S. B. *Macromolecules* **2006**, *39*, 6686.
(58) Welch, P. M.; Welch, C. F. *Macromolecules* **2009**, *42*, 7571.
(59) Allen, M. P.; Tildesley, D. J. *Computer Simulation of Liquids*; Clarendon Press: Oxford, UK, 1987.
(60) Press, W. H.; Teukolsky, S. A.; Vetterling, W. T.; Flannery, B. P. *Numerical Recipes in C*; Cambridge University Press: New York, 1994.
(61) Sheng, Y.-J.; Jiang, S.; Tsao, H.-K. *Macromolecules* **2002**, *35*, 7865.
(62) Kröger, M.; Peleg, O.; Halperin, A. *Macromolecules* **2010**, *43*, 6213.
(63) Ding, Y.; Öttinger, H. C.; Schlüter, A. D.; Kröger, M. *J. Chem. Phys.* **2007**, *127*, 094904.
(64) Kröger, M.; Peleg, O.; Ding, Y.; Rabin, Y. *Soft Matter* **2008** *4*, 18.